Supporting Information for

B-Site Tuned Curie Temperature and Band Gap in Half-Metallic $LaCu_3B_2Re_2O_{12}$ (*B* = Fe, Co, Ni) Quadruple Perovskite Oxides

Shuai Tang[1,2], Zhehong Liu[1], Alexey V. Ushakov[3], Fedor Temnikov[3], Xubin Ye[1], Zhao Pan[1], Chien-Te Chen[4], Chang-Yang Kuo[4,5], Zhiwei Hu[6], Sergey V. Streltsov[3,*] and Youwen Long[1,2,*]

AFFILIATIONS

[1]Beijing National Laboratory for Condensed Matter Physics, Institute of Physics, Chinese Academy of Sciences, Beijing 100190, China

[2]School of Physical Sciences, University of Chinese Academy of Sciences, Beijing 100049, China

[3]Institute of Metal Physics, Ekaterinburg 620108, Russia

[4]National Synchrotron Radiation Research Center, Hsinchu 30076, Taiwan

[5]Department of Electrophysics, National Yang Ming Chiao Tung University, Hsinchu 30010, Taiwan

[6]Max Planck Institute for Chemical Physics of Solids, Dresden 01187, Germany

*Corresponding Emails: streltsov@imp.uran.ru; ywlong@iphy.ac.cn

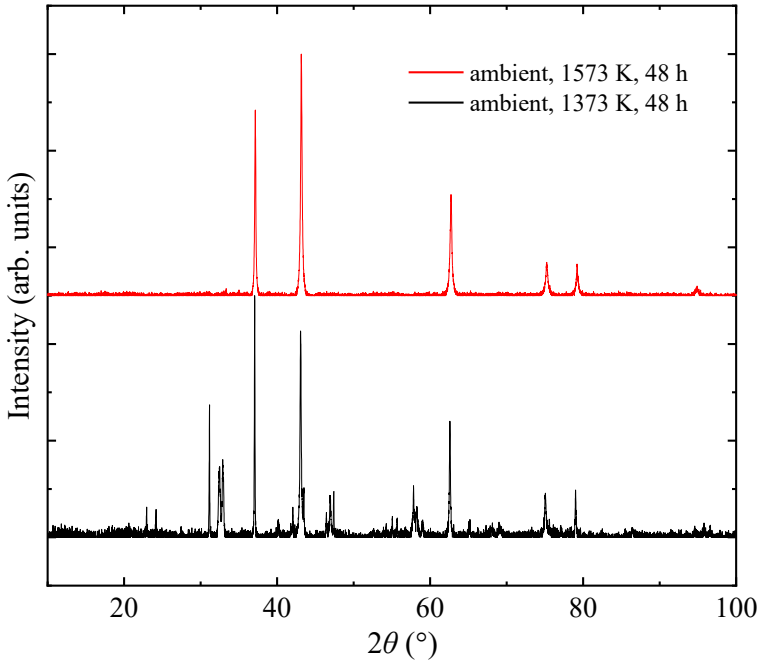

Fig. S1 Powder X-ray diffraction spectra of failed ambient-pressure attempts.

For the sample synthesized at 1373 K, the dominant phases identified by powder X-ray diffraction are $LaCuO_3$, La_2CuO_4, and NiO; under this condition rhenium species were observed to vaporize. At 1573 K the bulk residue consists primarily of $Cu_{0.2}Ni_{0.8}O$. We also observed that La-Cu containing products melted upon reaching their melting point and adhered to the inner wall of the crucible; rhenium was likewise lost from the bulk, consistent with volatilization and re-deposition on cooler parts of the reaction assembly.

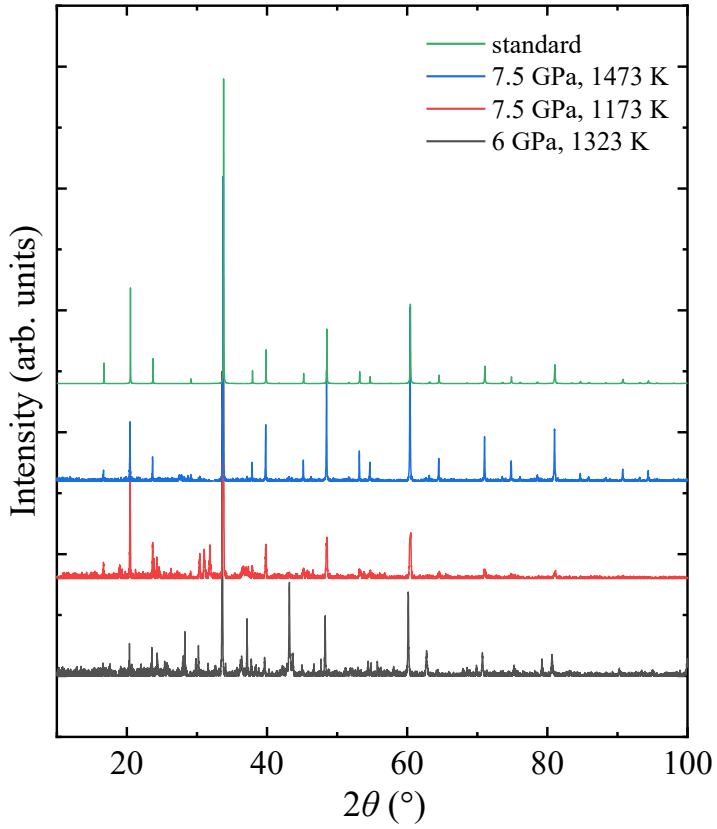

Fig. S2 Powder X-ray diffraction spectra under different conditions.

The powder X-ray diffraction data summarize samples prepared under varying pressure and temperature conditions. At lower pressure (6 GPa, 1323K) the reaction is incomplete, likely due to insufficient pressure to stabilize the target phase. At 7.5 GPa we initially employed a lower temperature (≈ 1173 K), relying on pressure to promote the reaction, but the diffraction pattern still show some intermediate impurity phases. Increasing the temperature at 7.5 GPa reduces some impurities, yet minor secondary reflections (e.g., near $2\theta \approx 30°$) remain, suggesting the pressure is still inadequate. When using 9 GPa at 1323 K (the conditions reported in the manuscript) we can obtain a phase-pure sample.

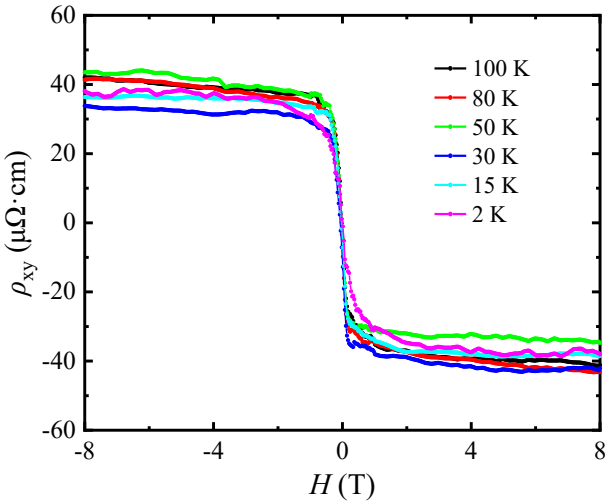

Fig. S3 Field-dependent Hall resistivity measured at different temperatures.

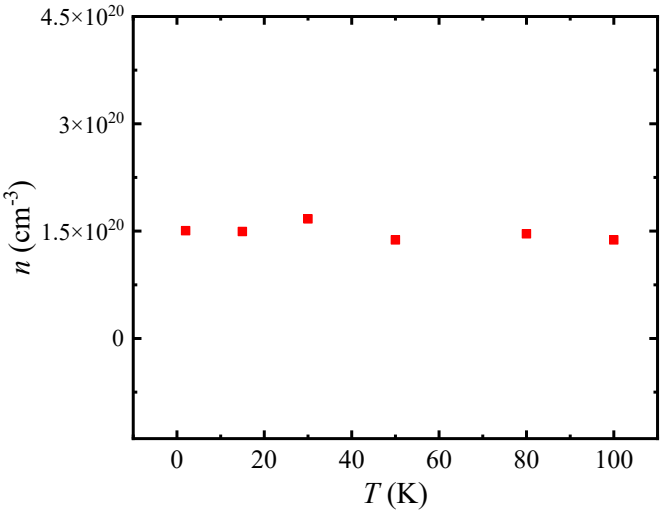

Fig. S4 Temperature dependence of the carrier concentration.

The sample for Hall effect measurements was polished to a thickness of about 220 μm (further thinning caused sample damage for our polycrystalline sample). To determine the carrier type, we analyzed the high-field region where the magnetization saturates. In this linear regime, the slope of the Hall resistivity ($d\rho_{xy}/dH$) is negative, indicating electron-like majority carriers. From linear fits to this high-field region, we extracted the ordinary Hall coefficient R_H, which yields an effective carrier concentration (n) on the order of 1.5×10^{20} cm^{-3}, as shown in Fig. S4. This value is relatively constant across the measured temperature range and is consistent with an intrinsically metallic electronic structure with relatively weak/low carrier density[1-4].

CALCULATION DETAILS

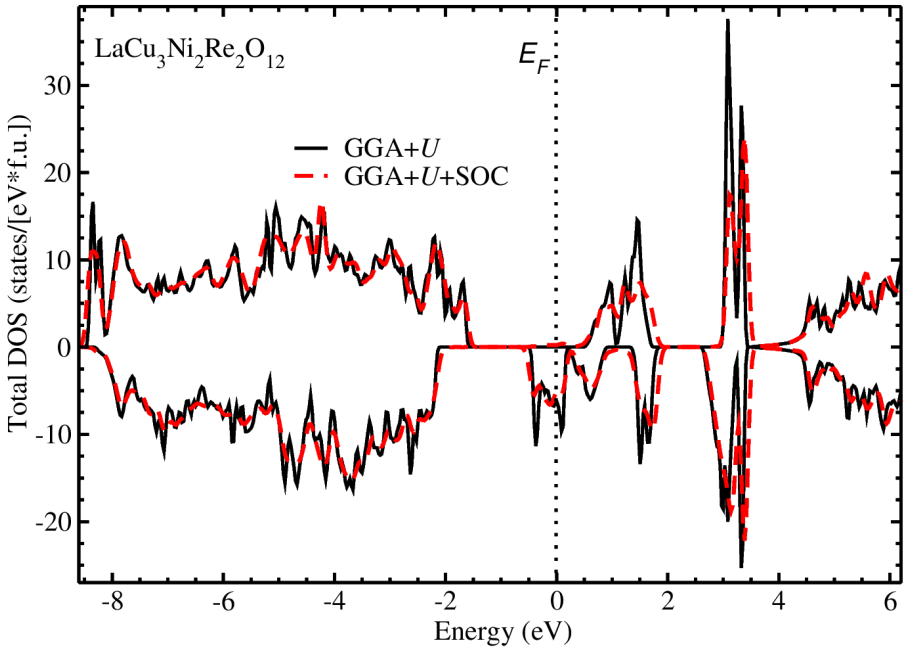

Fig. S5 Total DOS calculation using the GGA+*U* and GGA+*U*+SOC method.

The spin-polarized electronic structure calculations were performed using the full-potential linearized augmented plane-wave (FP-LAPW) method as implemented in WIEN2K. The convergence criteria were set to 0.000001 Ry for total energy and 0.000001 electrons for total charge. The initial magnetic configuration was chosen as a collinear antiferromagnetic state with Cu and Ni moments aligned parallel (↑) and Re moments antiparallel (↓). As shown in Fig. S5, the inclusion of SOC does not affect the ground state obtained with the GGA+*U* method. Subsequently, we discuss the GGA+*U* results. The optimization of the crystal structure using GGA+*U*(+SOC) clearly shows that the ions are already located in high-symmetry positions, with shifts in atomic positions (predominantly of oxygen) being negligibly small. Therefore, one may conclude that the ab-initio calculations confirm the experimental structure as largely applicable for LCNRO. The on-site Coulomb repulsion parameters were set to U = 8 eV for Cu, 6 eV for Ni, and 2 eV for Re. The Hund's rule coupling parameters were set to J_H = 0.9 eV for Cu and Ni, and 0.5 eV for Re. These U and J_H values follow previous studies[5-7]. The GGA+*U* calculations employed the Fully Localized Limit (FLL) double-

counting correction scheme (SIC method). Brillouin-zone sampling used a uniform grid amounting to 1000 *k*-points in the full Brillouin zone (76 *k*-points in the irreducible part). A plane-wave energy cutoff of −6.0 Ry was used. Semicore states La-5*p* and Cu-3*p* were treated as valence states.

REFERENCES

(1) Okuda, T.; Nakanishi, K.; Miyasaka, S.; Tokura, Y. Large Thermoelectric Response of Metallic Perovskites: $Sr_{1-x}La_xTiO_3$ ($0 \leq x \leq 0.1$). *Phys. Rev. B* **2001**, *63*, 113104.

(2) Spinelli, A.; Torija, M. A.; Liu, C.; Jan, C.; Leighton, C. Electronic Transport in Doped $SrTiO_3$: Conduction Mechanisms and Potential Applications. *Phys. Rev. B* **2010**, *81*, 155110.

(3) Beveren, L. W. van; Panchenko, E.; Anachi, N.; Hyde, L.; Smith, D.; James, T.; Roberts, A.; McCallum, J. Indium Tin Oxide Film Characterization Using the Classical Hall Effect. *arXiv* **2015**, 1503.03679.

(4) Kim, D.; Lee, S. Persistent Metallic Sn-Doped In_2O_3 Epitaxial Ultrathin Films with Enhanced Infrared Transmittance. *Sci. Rep.* **2020**, *10*, 4957.

(5) Sun, L.; Han, J.; Ge, Q.; Zhu, X.; Wang, H. Understanding the Role of Cu^+/Cu^0 Sites at Cu_2O Based Catalysts in Ethanol Production from CO_2 Electroreduction - A DFT Study. *RSC Adv.* **2022**, *12*, 19394.

(6) Been, E.; Lee, W.-S.; Hwang, H. Y.; Cui, Y.; Zaanen, J.; Devereaux, T.; Moritz, B.; Jia, C. Electronic Structure Trends Across the Rare-Earth Series in Superconducting Infinite-Layer Nickelates. *Phys. Rev. X* **2021**, *11*, 011050.

(7) Lim, T.-W.; Kim, S.-D.; Sung, K.-D.; Rhyim, Y.-M.; Jeen, H.; Yun, J.; Kim, K.-H.; Song, K.-M.; Lee, S.; Chung, S.-Y.; Choi, M.; Choi, S.-Y. Insights into Cationic Ordering in Re-Based Double Perovskite Oxides. *Sci. Rep.* **2016**, *6*, 19746.